

# Journal of Materials Chemistry A

Accepted Manuscript



This is an *Accepted Manuscript*, which has been through the Royal Society of Chemistry peer review process and has been accepted for publication.

*Accepted Manuscripts* are published online shortly after acceptance, before technical editing, formatting and proof reading. Using this free service, authors can make their results available to the community, in citable form, before we publish the edited article. We will replace this *Accepted Manuscript* with the edited and formatted *Advance Article* as soon as it is available.

You can find more information about *Accepted Manuscripts* in the [Information for Authors](#).

Please note that technical editing may introduce minor changes to the text and/or graphics, which may alter content. The journal's standard [Terms & Conditions](#) and the [Ethical guidelines](#) still apply. In no event shall the Royal Society of Chemistry be held responsible for any errors or omissions in this *Accepted Manuscript* or any consequences arising from the use of any information it contains.

# Modelling and Simulation of Electron-Rich Effect on the Li Diffusion in Group IVA Elements (Si, Ge and Sn) for Li Ion Batteries

Zhiguo Wang,<sup>1\*</sup> Qiulei Su,<sup>2</sup> Huiqiu Deng,<sup>2</sup> Weidong He,<sup>3</sup> Junhao Lin,<sup>4</sup> and Y.Q. Fu<sup>5</sup>

*1 School of Physical Electronics, Joint Laboratory for Police Equipment Research, University of Electronic Science and Technology of China, Chengdu, 610054, P.R. China*

*2 Department of Applied Physics, Hunan University, Changsha 410082, P.R. China*

*3 School of Energy Science and Engineering, University of Electronic Science and Technology of China, Chengdu 611731, PR China*

*4 Department of Physics and Astronomy, Vanderbilt University, Nashville, TN 37235, USA*

*5 Thin Film Centre, Scottish Universities Physics Alliance (SUPA), University of the West of Scotland, Paisley PA1 2BE, UK*

\*Corresponding author. E-mail: [zgwang@uestc.edu.cn](mailto:zgwang@uestc.edu.cn)

**ABSTRACT:** Improvement in electrical conductivity and lithium (Li) mobility for Li ion batteries is of particular importance for their high-power applications. Electron energy loss spectroscopy mapping shows that electrochemical reaction front region is under an electron-rich condition during lithiation. In this paper, electron-rich effect on diffusion behaviors of Li in pristine and phosphorus-doped group IVA elements, e.g., silicon, germanium and tin, were investigated using first principles density functional theory (DFT) calculations in combination with climbing-image nudged elastic band and *ab initio* DFT molecular dynamics. Phosphorus doping was found not a critical factor for enhanced Li diffusion into Si. Instead, results showed that the diffusion barriers and diffusivity of Li are mainly affected by electron-rich effect, i.e., the energy barriers decrease and diffusivity increases in an electron-rich environment. The decreases in diffusion barriers were attributed to the relaxation of the Si-Si bonds with extra electrons, which can also apply to the case of Ge, but not for the case of metallic Sn. Our new

findings provide a theoretical and experimental basis for design and fabrication of next generation batteries with a high power density.

**KEYWORDS:** Electron-rich, Li diffusion, anode materials, density functional calculations

## 1. INTRODUCTION

Among various electrochemical energy storage systems, lithium-ion batteries (LIBs) are increasingly attractive for stationary renewable energy resources and have been one of the leading power sources for electric vehicles. However, the current LIBs technology cannot meet the rapidly-increasing power demand, therefore to further improve the overall battery performance, various types of materials have been employed to design and fabricate the state-of-art LIBs<sup>1-3</sup>. These materials are required to have high volumetric energy and power density, limited environmental impact and long cycling life.<sup>4</sup> Group IVA (Si, Ge, and Sn) elements are potential anode materials for the LIBs<sup>1,5-9</sup>, due to their large gravimetric capacity<sup>10, 11</sup>. One major drawback of anodes made of the Group IVA elements is the large volume change during lithiation, for example, volume change can be up to 400% after Li<sup>+</sup> ion insertion and formation of Li<sub>x</sub>Si alloys for Si anode<sup>12</sup>. As the Li<sup>+</sup> ions are extracted during operation, the drastic volume shrinkage could lead to cracking and pulverization of the anodes. Tremendous efforts have been made to overcome this problem and improve cycling performance by decreasing the size of the anode materials, coating the anode with nano-structured Si based materials (Si nanowires and Si-C nano-composites)<sup>13</sup>, or alloying with active/inactive elements<sup>14</sup>. It is well documented that the electrochemically driven insertion of lithium ions into the semiconductor will lead to amorphization of the anode<sup>15, 16</sup>. Recently, Wang et al.<sup>17</sup> investigated the mechanisms of amorphization of Li-Si alloys formed during the electrochemical lithiation of crystalline Si using

both theoretical simulations and *in-situ* transmission electron microscopy (TEM). They concluded that electron-rich effect plays an important role in the electrochemical solid-state amorphization.<sup>17</sup> In Ref [17], the lithiation process of Si nanowires were analyzed using Z-contrast imaging and *in-situ* mapping from electron energy loss spectroscopy (EELS) mapping, the distribution maps of Li and Si were identified with the EELS using an aberration corrected STEM. As shown in Fig. 1 (a), Si core showed higher Z-contrast compared to the outer  $\text{Li}_x\text{Si}$  shell. The distribution maps of Li, Si, and overlaid Li and Si composite showed an enhanced  $\text{Li}^+$  concentration maximum at the interface between  $\text{Li}_x\text{Si}$  and Si. In order to remain the charge balance of the system, the enrichment of  $\text{Li}^+$  concentration at the interface between  $\text{Li}_x\text{Si}$  and Si leads to the portion of the Si core to have a higher electron density as illustrated by a schematic model in Fig. 1 (b). Therefore, the reaction front region is under an electron-rich condition during lithiation. Study of electron-rich effect on the diffusion of Li is important for development of high power density LIBs.

To improve the electron conductivity and ion diffusivity of the Si anodes, carbon coating and doping are commonly used. Chen et al.<sup>18</sup> found that phosphorus-doped Si film exhibit an improved rate performance. Using *in-situ* TEM, Liu et al.<sup>19</sup> showed that carbon coating and phosphorus doping resulted in an increase of 2~3 orders of magnitude in electrical conductivity of the Si, and an order of magnitude increase in its charging rate. Yi et al.<sup>20</sup> showed that the rate capability of Si-C composite can be enhanced by facile boron doping. However, the mechanism of the doping effect on the charging rate is not well understood. In order to make new generation batteries using Si, Ge, and Sn as anode materials, understanding the diffusion of Li within these materials is of fundamental importance. First principle computational studies have been carried out to study the diffusion of Li ions in bulk crystalline Si,<sup>21</sup> Si thin films,<sup>22,23</sup> and Si nanowires,<sup>24</sup>

<sup>25</sup>, as well as the orientation dependent lithiation of Si.<sup>26</sup> However, these studies did not provide detailed insights into the mechanisms of enhanced mobility of Li and doping effect on the charging rate. In this paper, for the first time, we present in-depth analysis of electron-rich and doping effects on the diffusion of Li in Si, Ge and Sn based on density functional theory (DFT). We concluded that the energy barriers of Li diffusion are significantly reduced with the addition of extra electrons into the system, which leads to a fast charging of Li into the anode material. Our results could provide a theoretical basis for the design and fabrication of next generation batteries with a high power density.

## 2. CALCULATION METHODS

Migration of Li in the Si, Ge and Sn materials were investigated using density functional theory calculations as implemented in the Vienna *ab initio* package (VASP)<sup>27</sup>. The projector augmented wave (PAW) method<sup>28</sup> was used to describe electron-ion interaction, and the generalized gradient approximation based on the Perdew-Burke-Ernzerhof (PBE) function was used to describe the electron exchange-correlation. A plane wave basis was set up to an energy cutoff of 400 eV. Si and Ge have a diamond-type crystal structure, while Sn has a body centered tetragonal structure ( $\beta$ -Sn) at ambient temperature and pressure. Computations were based on a  $2\times 2\times 2$  supercell (consisting of 64 atoms) with a  $2\times 2\times 2$  Monkhorst-Pack<sup>29</sup> mesh for the  $k$ -point sampling for Si and Ge. A  $4\times 4\times 4$   $k$ -mesh caused the total energy of the system to converge within 0.02 eV, which indicates that a  $2\times 2\times 2$   $k$ -mesh should provide a well converged result. As phosphorus (P) doping can result in the increase of charging rate, the effect of P-doping on the diffusion of Li atoms was also investigated using the same  $2\times 2\times 2$  supercell with one Si atom substituted by one atom of P. A  $3\times 3\times 3$  supercell (consisting of 108 atoms) was used to study the

diffusion of Li in Sn. Each saddle point structure and its associated minimum energy pathway were computed using a climbing-image nudged elastic band (CI-NEB) method<sup>30</sup>. Following the optimization of all degrees of freedom in each structure, the search of transition state began with a nudged elastic band (NEB) calculation, which involved a chain of images (seven in the present calculations) determined through a linear interpolation from the fixed initial and final configurations. The electron-rich effects on the diffusion of Li in the Si, Ge and Sn were studied, and extra numbers of electrons ( $N_e$ ) were added into the Si/Ge/Sn lattices to characterize the modified electron density. For the Si and Ge, the model contained 64 Si atoms contributing 256 electrons, and value of  $N_e=1/64$  was used to denote the modified electron density when four electrons were added to the system. We set  $N_e=1/64$ ,  $1/32$ , and  $3/64$  to investigate the effect of extra electrons on the diffusion of Li and Na. For the metallic Sn, we studied effect of electron density of  $N_e=1/108$ ,  $1/54$ , and  $1/36$  on the diffusion of Li.

The lithiation of Si under electron rich condition was also investigated using *ab initio* molecular dynamics calculations within the framework of DFT as in the SIESTA code<sup>31</sup>, which adopts a linear combination of numerical localized atomic orbital basis sets for the description of valence electrons and norm-conserving nonlocal pseudopotentials for the atomic core<sup>32</sup>. The valence electron wave functions were expanded using a double- $\zeta$  basis set. The charge density was projected on a real space grid with a cutoff of 150 Ry to calculate the self-consistent Hamiltonian matrix elements, and  $\Gamma$  point was used in the Brillouin zone sampling. The evolution of the system was derived using the molecular dynamics (MD) method with a verlet algorithm for all the atoms after adding extra electrons, and a time-step of 1.0 fs. Fermi distribution was used for the added electronic charges to be placed into the empty states. The same scheme was used to simulate mixing process of Li with Si<sup>33</sup>: as the volume of Si-anode in

the LIBs was expanded after lithiation with an expansion ratio of  $\sim 60\%$  at  $0\text{ K}^{33}$ , a  $3\times 3\times 2$  supercell (consisting of 144 Si atoms) of crystalline Si was selected with increasing the supercell in  $z$ -direction by 60%. The space above the silicon was initially filled with 144 amorphous Li atoms. Starting from the initial configuration, the atom positions were relaxed at a given temperature with 15000 MD steps. The time of 15 ps was proved sufficient for mixing of the Li and Si atoms. To accelerate the lithiation process, high temperatures of 1100, 1200, 1300, 1400 and 1500 K with  $N_e=0, 3/64$  and  $5/64$  were applied. Mean square displacements (MSD) for the Li and Si atoms as a function of time were calculated to compute diffusivities of Li and Si at different temperatures, which were then extrapolated to obtain diffusivities of the Li and Si at room temperature. The *ab initio* MD calculations took almost half a year to finish with twenty central processing units in parallel computation.

### 3. RESULTS AND DISCUSSION

To study the diffusion pathway of Li in Si/Ge/Sn, the stable configurations of the Li atoms inside the Si/Ge/Sn lattices are to be determined. Different nonequivalent positions (tetrahedral site, hexagonal site, anti-bonding site and bond-center) of the Li in the lattice of the Si/Ge/Sn have been examined<sup>34</sup>. The tetrahedral interstitial site ( $T_d$  symmetry) is the most stable form of interstitial Li in both the Si and Ge, as shown by the red balls in Fig. 2 (a). It has four nearest-neighbor Si/Ge atoms and six second-nearest-neighbor Si/Ge atoms with Li-Si and Li-Ge distances of 2.445 Å and 2.585 Å, respectively. The most stable position for an interstitial Li in  $\beta$ -Sn is shown by the red ball in Fig. 2 (b), which is enclosed by five Sn atoms with a bond length between 2.00 and 2.73 Å. The diffusion process consists of moving away of the Li atoms from one stable position to a neighboring position by passing through a hexagonal or a rhombus

interstitial site in Si/Ge or  $\beta$ -Sn, respectively, as shown by the blue balls in Figs. 2 (a) and (b). At the hexagonal interstitial (Hex) site, the Li has six nearest neighboring Si/Ge atoms, and their configurations can be viewed as two parallel triangles, both of which are perpendicular to the diffusion pathway. At the rhombus interstitial site in the  $\beta$ -Sn, Li has two nearest-neighboring Sn atoms and two second-nearest-neighboring Sn atoms, with Li-Sn distances of 2.577 and 2.728 Å, respectively.

Fig. 3 shows the diffusion barrier of Li atoms in the Si, Ge, Sn and P-doped Si through the as-mentioned migration pathway (two adjacent  $T_d$  sites). For the neutral state with  $N_e=0$ , the calculated energy barriers for Li diffusion in Si and Ge are about 0.57 eV and 0.39 eV, respectively, which are in agreement with the previous theoretical calculations.<sup>35-37</sup> The energy barrier for Li diffusion in Sn is about 0.39 eV, and 0.53 eV in P-doped Si. However, recent experiments showed that the lithiation speed of Li diffusion inside the highly phosphorous-doped Si-NWs was about  $\sim 200$  times that of the intrinsic Si-NWs<sup>19</sup>. The similar diffusion barriers of the Li atoms in intrinsic and P-doped Si from our analysis suggest that the phosphorus atoms may not play a key role in the increased lithiation speed, but P doping will enhance the conductivity of electron, thus making electron rich environment between the interface Si and Li.

Fig. 3(a) shows the energy profiles of Li migrations along the  $T_d$ -Hex- $T_d$  pathway with extra electrons in the pristine Si. In the presence of additional electrons, the diffusion barriers of Li in the pristine Si are reduced. For example, the energy barrier of Li atom decreases by  $\sim 0.2$  eV as electrons of  $N_e=3/64$  are added into the system. The diffusion coefficient varies exponentially with the diffusion barrier following an Arrhenius-like formula<sup>38</sup>:  $D \propto e^{-E_A/k_B T}$ , where  $E_A$  is the diffusion energy barrier,  $k_B$  the Boltzmann constant and  $T$  the temperature. Therefore, the reduction of energy barrier (0.2 eV) could change the Li mobility by a factor of  $\sim 3000$  at room

temperature. Therefore, it is clear that the diffusion of Li can be enhanced by adding extra electrons into the system. The reduction of the diffusion barrier can also be achieved in Ge and Sn with added extra electrons, as shown in Figs. 3 (b) and (c), respectively. However, the reduction of the diffusion barrier in Sn is not as significant as those in the Si and Ge, e.g., the reductions are found to be 0.2, 0.1 and 0.05 eV for Li in the Si, Ge and Sn, respectively, using a value of  $N_e \approx 1/32$ . Fig. 3 (c) also shows the saddle point of  $N_e=1/36$  is higher than that of  $1/54$ . The differences can be explained from the electron conduction mechanisms of these materials, i.e., Si and Ge are semiconductors whereas Sn is metallic. In the Si and Ge, the bonds are covalent, whereas the bond in  $\beta$ -Sn is metallic. The electrons filling up the anti-bonding  $sp^3$  of the covalent bond soften the Si-Si/Ge-Ge bonds. In addition, the diffusion barriers of the Li can be further reduced if the same amount of extra electrons are added to the P-doped Si, as shown in Fig. 3 (d), i.e. the energy barrier of Li atom decreases by 0.27 eV when electrons of  $N_e=3/64$  are added into the P-doped Si system. These results clearly indicate that the acceleration of electron accumulation at the interface of Si/Li, which forms an electron-rich environment, plays a dominant role in the lithiation process. Moreover, P-doping enhances transportation of electrons and improves electron conductivity of the Si, resulting in accumulation of more electrons at the Si/Li interface, and increase of the lithiation of Si.

We also studied the changes of bond lengths when the Li is located at the saddle point of Si. The bond lengths of Si-Si and Li-Si of the puckered hexagon increase with increasing the value of  $N_e$ . Table 1 lists the calculated bond lengths of Si-Si, Li-Si, Ge-Ge and Li-Ge, respectively. The expansion of lattice can promote Li diffusion in the lattices. The charge redistribution caused by the Li insertion in the saddle point can be studied from the differences in charge densities on the plane containing the Li and neighbor Si atoms via the equation (1),

$$\Delta\rho(\mathbf{r}) = \rho_{Li\_Si}(\mathbf{r}) - \rho_{Li}(\mathbf{r}) - \rho_{Si}(\mathbf{r}) \quad (1)$$

where  $\rho_{Li\_Si}(\mathbf{r})$  is the charge density of the Li at the Hex site of the Si system,  $\rho_{Si}(\mathbf{r})$  and  $\rho_{Li}(\mathbf{r})$  are the electron charge densities of the bulk Si and an isolated Li at the same position as in the systems, respectively. The charge density differences for Ne=0, 1/64, 1/32, and 3/64 are shown in Fig. 4. The yellow surfaces correspond to charge gains and the cyan surfaces correspond to loss of an equivalent charge. The electronic charge across the neighboring Si-Si bond decreases, resulting in a net loss of electronic charge of Li as well as an increase of the electronic charge in the Li-Si bond. The decrease of electronic charge across the neighboring Si-Si bond is caused by the increase of the length of the Si-Si bond, which results in the decrease in the Li-Si interaction. It is also noticed that the blue surface surrounding Li decreases with increasing additional electrons and the net loss of electronic charge of Li decreases. Therefore, the interactions between Li and the surrounding Si atoms will be weakened, facilitating the diffusion of Li through the Hex site.

The diffusion properties were also determined by *ab initio* MD calculations. During mixing of Li with Si, the positions  $r_i(t)$  of all the atoms at a time  $t$  were recorded. The corresponding mean square displacements (MSDs) per atom were calculated using the equation (2):

$$MSD = \langle |r_i(t) - r_i(0)|^2 \rangle = \frac{1}{N} \sum_{i=1}^N |r_i(t) - r_i(0)|^2 \quad (2)$$

where  $N$  is the total atomic number and ' $\langle \dots \rangle$ ' denotes the average value over all the atoms. The diffusion coefficient ( $D$ ) at a given temperature was determined using the Einstein relation:

$$D = \lim_{t \rightarrow \infty} \frac{MSD}{q_i t} = \lim_{t \rightarrow \infty} \frac{1}{q_i t} \langle |r_i(t) - r(0)|^2 \rangle \quad (3)$$

where  $q_i$  is a numerical constant which depends on the dimensionality; and  $q_i = 2, 4,$  or  $6$  describes one-, two- or three-dimensional diffusions, respectively. The relationship between the diffusion energy barrier ( $E_A$ ) and  $D$  is based on the Arrhenius equation<sup>38</sup>:

$$D = D_0 \exp(-E_A / k_B T). \quad (4)$$

The values of  $E_A$  and  $D$  were obtained by fitting the diffusion coefficient to the data obtained using equation (4) at different temperatures.

Starting from the initial configurations at  $t = 0$  ps as shown in Fig. 5, the atom positions were relaxed at a given temperature for 15000 MD time steps (15 ps). In Fig. 5, several snapshots of the structural evolution are shown as a function of time for the Li-Si system at 1200 K with  $N_e=0, 3/64,$  and  $5/64$ . The crystalline Si was found to transform into amorphous phase upon the electrochemical insertion of Li atoms. The Li atoms were observed to insert gradually into the Si-Si lattice by breaking or expanding the Si-Si bonds. The lithiation speed increased with increasing the numbers of electrons into the system, i.e., the dotted rectangles for simulation time of 1.2 ps. At a simulation time of 10 ps, the Li and Si atoms were fully mixed, which indicates that 15 ps is sufficient enough for substantial mixing of both the Li and Si atoms.

The calculated average values of the MSDs for the Li and Si atoms as a function of simulation time at different temperatures are shown in Fig. 6. As expected, the values of the MSDs increase linearly with the simulation time. However, the slope increases with the temperature, indicating a faster Li and Si atoms process at a higher temperature. The increase of the MSDs for Si is slower than that of the Li. The diffusivities at room temperature (i.e., 300 K) are shown in Fig. 7, which was obtained by extrapolating the data of diffusivities of Li and Si at different temperatures. The diffusion barrier ( $E_A$ ) and diffusion coefficients ( $D$ ) at 300 K obtained using Equation (4) are listed in Table 2.

The energy barrier for Li diffusion in Si calculated from Equation (4) is 0.75 eV, which is larger than the value of 0.57 eV calculated by the NEB method as shown in Fig. 2 (a). This could be explained by the fact that during the mixing of Li and Si, transition from crystalline to amorphous phases occurs (see Fig. 5). Therefore the calculated energy barrier of 0.75 eV is actually the value of Li diffusion into amorphous Si or a mixture of crystalline and amorphous phases, but not the exactly value of Li diffusion in the crystalline ones. The NEB results showed that the energy barrier of Li in the amorphous Si is in the range between 0.1 eV and 2.4 eV, and the most pathways in the amorphous Si have energy barriers higher than those for Li diffusion in the crystalline Si. This suggested that the diffusivity of Li in the amorphous Si should be smaller than that in crystalline Si<sup>39</sup>. The diffusivity of Li in the crystalline Si was calculated to be  $4.92 \times 10^{-14} \text{ cm}^2 \text{ s}^{-1}$  as shown in Table 2 with Ne=0. Experimental data of the diffusivity of Li in Si are in the range between  $10^{-14}$  and  $10^{-8} \text{ cm}^2 \text{ s}^{-1}$ <sup>40-46</sup>. Our result is close to the reported minimum diffusivity, which is mainly attributed to the electron rich effect. Our result also reveals that the diffusivity of Si is four orders of magnitude smaller than that of the Li, which suggests that the Si atoms are relatively stationary during the lithiation process. From Table 2, the energy barriers decrease and the diffusivity increases with adding more electrons into the system. The diffusivity of Li increases to  $1.05 \times 10^{-11} \text{ cm}^2 \text{ s}^{-1}$  with Ne=5/64, which is in a good agreement with the results of  $2 \times 10^{-11} \text{ cm}^2 \text{ s}^{-1}$  reported by Yoshimura et al., who used bipolar cells of Li in a single crystal Si plate<sup>43</sup>.

Results from both the DFT and *ab initio* DFT molecular dynamics showed that the electron-rich effect is a key mechanism controlling the diffusivity of Li and Si upon lithiation. In order to investigate the distribution of the added electrons in the lattice, we calculated the charge density difference using  $\Delta\rho(\mathbf{r}) = \rho^e(\mathbf{r}) - \rho^0(\mathbf{r})$ , where  $\rho^e$  and  $\rho^0$  are the charge density of Li-Si

systems with and without extra electrons, respectively. Results are shown in the inset of Fig. 6. The extra electrons are predominantly distributed at the Si part for both  $N_e=3/64$  and  $N_e=5/64$ . Electron-rich effect enhances the diffusivities of Li in Si and Ge due to the relaxation of Si-Si/Ge-Ge bonds filled up the anti-bonding  $sp^3$  states of Si/Ge with excessive electrons. The Si/Ge network is, therefore, destabilized by lithiation, which makes the diffusion of Li much easier.

#### 4. CONCLUSION

In summary, the diffusion behaviors of the Li in the pristine and P-doped Si, Ge and Sn were investigated using first principles density functional theory (DFT) calculations in combination with climbing-image nudged elastic band and *ab initio* DFT molecular dynamics. Results showed that the diffusion barriers of Li are 0.57 eV and 0.53 eV in pristine and P-doped silicon, suggesting that the diffusion is not apparently affected by the P-doping, but due to the electron rich effect. The energy barriers for the Li diffusing into lattices decrease with adding additional electrons into the system. The diffusivity of Li in Si is in the range between  $4.92 \times 10^{-14}$  and  $1.05 \times 10^{-11} \text{ cm}^2 \text{ s}^{-1}$ , which agrees well with the reported experiment data. Electron-rich effect also induces the decrease of diffusion barriers of Li in Ge and Sn. Results confirmed that an electron-rich effect plays a dominant role in the lithiation process, especially in semiconductors. This new finding provides a theoretical and experimental basis on the enhancement of charging rate by increasing the electron mobility in electrode materials.

#### Acknowledgement:

The authors thank the National Supercomputing Center in Changsha for providing the computing resources, and Royal Academy of Engineering UK-Research Exchange with China and India.

## References:

1. McDowell, M. T.; Lee, S. W.; Nix, W. D.; Cui, Y., 25th Anniversary Article: Understanding the Lithiation of Silicon and Other Alloying Anodes for Lithium-Ion Batteries. *Advanced Materials* 2013, 25, 4966-4985.
2. Xu, J.; Dou, S.; Liu, H.; Dai, L., Cathode materials for next generation lithium ion batteries. *Nano Energy* 2013, 2, 439-442.
3. Wagemaker, M.; Mulder, F. M., Properties and Promises of Nanosized Insertion Materials for Li-Ion Batteries. *Accounts of Chemical Research* 2012, 46, 1206-1215.
4. Tarascon, J. M.; Armand, M., Issues and challenges facing rechargeable lithium batteries. *Nature* 2001, 414, 359-367.
5. Gauthier, M.; Mazouzi, D.; Reyter, D.; Lestriez, B.; Moreau, P.; Guyomard, D.; Roue, L., A low-cost and high performance ball-milled Si-based negative electrode for high-energy Li-ion batteries. *Energy & Environmental Science* 2013, 6, 2145-2155.
6. Zamfir, M. R.; Nguyen, H. T.; Moyen, E.; Lee, Y. H.; Pribat, D., Silicon nanowires for Li-based battery anodes: a review. *Journal of Materials Chemistry A* 2013, 1, 9566-9586.
7. McDowell, M. T.; Ryu, I.; Lee, S. W.; Wang, C.; Nix, W. D.; Cui, Y., Studying the Kinetics of Crystalline Silicon Nanoparticle Lithiation with In Situ Transmission Electron Microscopy. *Advanced Materials* 2012, 24, 6034-6041.
8. Cho, Y. J.; Kim, C. H.; Im, H. S.; Myung, Y.; Kim, H. S.; Back, S. H.; Lim, Y. R.; Jung, C. S.; Jang, D. M.; Park, J.; Lim, S. H.; Cha, E. H.; Bae, K. Y.; Song, M. S.; Cho, W. I., Germanium-tin alloy nanocrystals for high-performance lithium ion batteries. *Physical Chemistry Chemical Physics* 2013, 15, 11691-11695.

9. Gu, Y.; Wu, F.; Wang, Y., Confined Volume Change in Sn-Co-C Ternary Tube-in-Tube Composites for High-Capacity and Long-Life Lithium Storage. *Advanced Functional Materials* 2013, 23, 893-899.
10. Park, C.-M.; Kim, J.-H.; Kim, H.; Sohn, H.-J., Li-alloy based anode materials for Li secondary batteries. *Chemical Society Reviews* 2010, 39, 3115-3141.
11. Kasavajjula, U.; Wang, C. S.; Appleby, A. J., Nano- and bulk-silicon-based insertion anodes for lithium-ion secondary cells. *J. Power Sources* 2007, 163, 1003-1039.
12. Chan, C. K.; Peng, H. L.; Liu, G.; McIlwrath, K.; Zhang, X. F.; Huggins, R. A.; Cui, Y., High-performance lithium battery anodes using silicon nanowires. *Nat. Nanotechnol.* 2008, 3, 31-35.
13. Szczech, J. R.; Jin, S., Nanostructured silicon for high capacity lithium battery anodes. *Energy & Environmental Science* 2011, 4, 56-72.
14. Abel, P. R.; Chockla, A. M.; Lin, Y.-M.; Holmberg, V. C.; Harris, J. T.; Korgel, B. A.; Heller, A.; Mullins, C. B., Nanostructured Si(1-x)Gex for Tunable Thin Film Lithium-Ion Battery Anodes. *ACS Nano* 2013, 7, 2249-2257.
15. Limthongkul, P.; Jang, Y. I.; Dudney, N. J.; Chiang, Y. M., Electrochemically-driven solid-state amorphization in lithium-silicon alloys and implications for lithium storage. *Acta Materialia* 2003, 51, 1103-1113.
16. Liu, X. H.; Wang, J. W.; Huang, S.; Fan, F.; Huang, X.; Liu, Y.; Krylyuk, S.; Yoo, J.; Dayeh, S. A.; Davydov, A. V.; Mao, S. X.; Picraux, S. T.; Zhang, S.; Li, J.; Zhu, T.; Huang, J. Y., In situ atomic-scale imaging of electrochemical lithiation in silicon. *Nat Nano* 2012, 7, 749-756.

17. Wang, Z.; Gu, M.; Zhou, Y.; Zu, X.; Connell, J. G.; Xiao, J.; Perea, D.; Lauhon, L. J.; Bang, J.; Zhang, S.; Wang, C.; Gao, F., Electron-Rich Driven Electrochemical Solid-State Amorphization in Li–Si Alloys. *Nano Letters* 2013, 13, 4511-4516.
18. Chen, X.; Gerasopoulos, K.; Guo, J.; Brown, A.; Ghodssi, R.; Culver, J. N.; Wang, C., High rate performance of virus enabled 3D n-type Si anodes for lithium-ion batteries. *Electrochimica Acta* 2011, 56, 5210-5213.
19. Liu, X. H.; Zhang, L. Q.; Zhong, L.; Liu, Y.; Zheng, H.; Wang, J. W.; Cho, J. H.; Dayeh, S. A.; Picraux, S. T.; Sullivan, J. P.; Mao, S. X.; Ye, Z. Z.; Huang, J. Y., Ultrafast Electrochemical Lithiation of Individual Si Nanowire Anodes. *Nano Letters* 2011, 11, 2251-2258.
20. Yi, R.; Zai, J.; Dai, F.; Gordin, M. L.; Wang, D., Improved rate capability of Si-C composite anodes by boron doping for lithium-ion batteries. *Electrochemistry Communications* 2013, 36, 29-32.
21. Wan, W. H.; Zhang, Q. F.; Cui, Y.; Wang, E. G., First principles study of lithium insertion in bulk silicon. *J. Phys.-Condes. Matter* 2010, 22.
22. Peng, B.; Cheng, F. Y.; Tao, Z. L.; Chen, J., Lithium transport at silicon thin film: Barrier for high-rate capability anode. *J. Chem. Phys.* 2010, 133.
23. Chou, C.-Y.; Hwang, G. S., Surface effects on the structure and lithium behavior in lithiated silicon: A first principles study. *Surface Science* 2013, 612, 16-23.
24. Zhang, Q. F.; Cui, Y.; Wang, E. G., Anisotropic Lithium Insertion Behavior in Silicon Nanowires: Binding Energy, Diffusion Barrier, and Strain Effect. *Journal of Physical Chemistry C* 2011, 115, 9376-9381.
25. Zhang, Q. F.; Zhang, W. X.; Wan, W. H.; Cui, Y.; Wang, E. G., Lithium Insertion In Silicon Nanowires: An ab Initio Study. *Nano Letters* 2010, 10, 3243-3249.

26. Chan, M. K. Y.; Wolverton, C.; Greeley, J. P., First Principles Simulations of the Electrochemical Lithiation and Delithiation of Faceted Crystalline Silicon. *J. Am. Chem. Soc.* 2012, 134, 14362-14374.
27. Kresse, G.; Furthmuller, J., Efficiency of ab-initio total energy calculations for metals and semiconductors using a plane-wave basis set. *Computational Materials Science* 1996, 6, 15-50.
28. Kresse, G.; Joubert, D., From ultrasoft pseudopotentials to the projector augmented-wave method. *Phys. Rev. B* 1999, 59, 1758-1775.
29. Pack, J. D.; Monkhorst, H. J., SPECIAL POINTS FOR BRILLOUIN-ZONE INTEGRATIONS - REPLY. *Phys. Rev. B* 1977, 16, 1748-1749.
30. Henkelman, G.; Uberuaga, B. P.; Jonsson, H., A climbing image nudged elastic band method for finding saddle points and minimum energy paths. *J. Chem. Phys.* 2000, 113, 9901-9904.
31. Soler, J. M.; Artacho, E.; Gale, J. D.; Garcia, A.; Junquera, J.; Ordejon, P.; Sanchez-Portal, D., The SIESTA method for ab initio order-N materials simulation. *Journal of Physics-Condensed Matter* 2002, 14, 2745-2779.
32. Troullier, N.; Martins, J. L., EFFICIENT PSEUDOPOTENTIALS FOR PLANE-WAVE CALCULATIONS. *Physical Review B* 1991, 43, 1993-2006.
33. Johari, P.; Qi, Y.; Shenoy, V. B., The Mixing Mechanism during Lithiation of Si Negative Electrode in Li-Ion Batteries: An Ab Initio Molecular Dynamics Study. *Nano Letters* 2011, 11, 5494-5500.
34. Wan, W.; Zhang, Q.; Cui, Y.; Wang, E., First principles study of lithium insertion in bulk silicon. *Journal Of Physics-Condensed Matter* 2010, 22.

35. Milman, V.; Payne, M. C.; Heine, V.; Needs, R. J.; Lin, J. S.; Lee, M. H., Free energy and entropy of diffusion by ab initio molecular dynamics: Alkali ions in silicon. *Physical Review Letters* 1993, 70, 2928-2931.
36. Wan, W. H.; Zhang, Q. F.; Cui, Y.; Wang, E. G., First principles study of lithium insertion in bulk silicon. *J. Phys.-Condes. Matter* 2010, 22, 415501.
37. Tritsarlis, G. A.; Zhao, K. J.; Okeke, O. U.; Kaxiras, E., Diffusion of Lithium in Bulk Amorphous Silicon: A Theoretical Study. *J. Phys. Chem. C* 2012, 116, 22212-22216.
38. Janz, G. J.; Kerbs, U.; Siegenthaler, H., Molten Salts: Volume 3 Nitrates, Nitrites, and Mixtures: Electrical Conductance, Density, Viscosity, and Surface Tension Data. *J. Phys. Chem. Ref. Data* 1972, 1.
39. Tritsarlis, G. A.; Zhao, K.; Okeke, O. U.; Kaxiras, E., Diffusion of Lithium in Bulk Amorphous Silicon: A Theoretical Study. *The Journal of Physical Chemistry C* 2012, 116, 22212-22216.
40. Ding, N.; Xu, J.; Yao, Y. X.; Wegner, G.; Fang, X.; Chen, C. H.; Lieberwirth, I., Determination of the diffusion coefficient of lithium ions in nano-Si. *Solid State Ionics* 2009, 180, 222-225.
41. Ruffo, R.; Hong, S. S.; Chan, C. K.; Huggins, R. A.; Cui, Y., Impedance Analysis of Silicon Nanowire Lithium Ion Battery Anodes. *The Journal of Physical Chemistry C* 2009, 113, 11390-11398.
42. Xie, J.; Imanishi, N.; Zhang, T.; Hirano, A.; Takeda, Y.; Yamamoto, O., Li-ion diffusion in amorphous Si films prepared by RF magnetron sputtering: A comparison of using liquid and polymer electrolytes. *Materials Chemistry and Physics* 2010, 120, 421-425.

43. Yoshimura, K.; Suzuki, J.; Sekine, K.; Takamura, T., Measurement of the diffusion rate of Li in silicon by the use of bipolar cells. *Journal of Power Sources* 2007, 174, 653-657.
44. Balke, N.; Jesse, S.; Kim, Y.; Adamczyk, L.; Tselev, A.; Ivanov, I. N.; Dudney, N. J.; Kalinin, S. V., Real Space Mapping of Li-Ion Transport in Amorphous Si Anodes with Nanometer Resolution. *Nano Letters* 2010, 10, 3420-3425.
45. Pell, E. M., Diffusion of Li in Si at High T and the Isotope Effect. *Physical Review* 1960, 119, 1014-1021.
46. Pell, E. M., Diffusion Rate of Li in Si at Low Temperatures. *Physical Review* 1960, 119, 1222-1225.

Table 1 Bond lengths (in Å) of Si-Si, Li-Si, Ge-Ge and Li-Ge when the Li is located at the saddle point of Si and Ge.

	Si-Si	Li-Si	Ge-Ge	Li-Ge
Ne=0	2.4671	2.3695	2.6003	2.5004
Ne=1/64	4.4676	2.3698	2.6009	2.5021
Ne=2/32	2.4689	2.3721	2.6016	2.5100
Ne=3/64	2.4700	2.3737	2.6030	2.5197

Table 2 Computed diffusion coefficients (in  $\text{cm}^2 \text{s}^{-1}$ ) and diffusion energy barriers (in eV) at 300 K.

	$D_{\text{Li}}$	$E_{\text{A}}(\text{Li})$	$D_{\text{Si}}$	$E_{\text{A}}(\text{Si})$
Ne=0	$4.92 \times 10^{-14}$	0.75	$1.42 \times 10^{-18}$	1.06
Ne=3/64	$2.64 \times 10^{-12}$	0.59	$3.80 \times 10^{-14}$	0.72
Ne=5/64	$1.05 \times 10^{-11}$	0.53	$1.17 \times 10^{-13}$	0.68

**Figure Captions:**

**Figure 1.** (a) STEM Z-contrast image, Li maps, Si maps, and Li/Si composite maps showing the distribution of Li and Si in different lithiation stages<sup>17</sup>. (b) Schematic drawing illustrating the distribution of Li and electrons during lithiation based on interface-controlled lithiation theory. Due to the interface-controlled lithiation process, Li accumulates at the interface and forms a Li<sup>+</sup> rich interface, while electrons are rich in the silicon core.

**Figure 2.** Atomic structures of diamond (a) Si and Ge, and (b) body centered tetragonal Sn. The green ball represents Si and Ge atoms. Cyan ball represents Sn. Red and blue balls represent the stable and transition state of Li atoms, respectively.

**Figure 3.** Energy profiles of Li diffuse in (a) pristine Si, (b) pristine Ge, (c) pristine Sn, and (d) P-doped Si with and without adding additional electron on the systems.

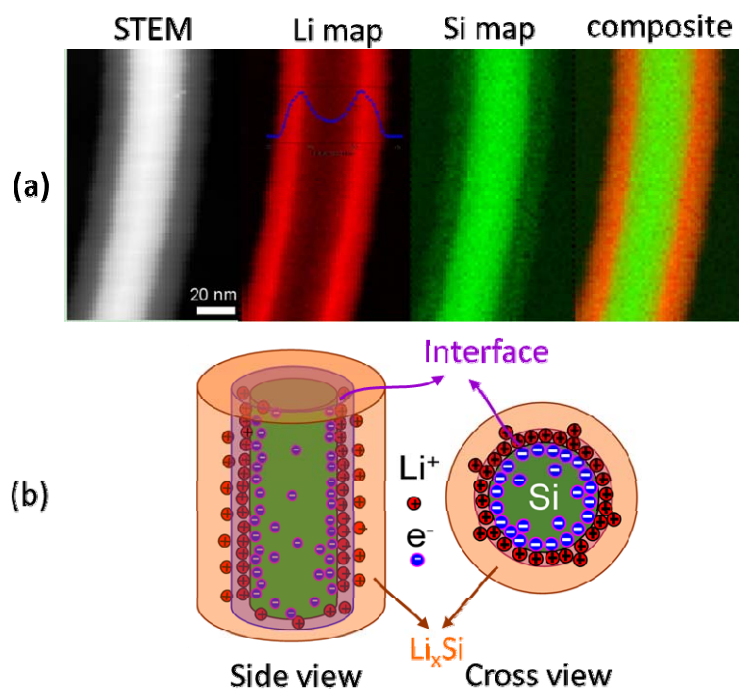
**Figure 4.** Isosurface of the charge density difference for Li located at saddle (Hex) site ( $0.0008 \text{ e}/\text{\AA}^3$ ) with adding additional electron of Ne=(a) 0, (b) 1/64, (c) 1/32, and (d) 3/64. Yellow surfaces correspond to charge gains and cyan surfaces correspond to an equivalent charge lost.

**Figure 5.** Structural snapshots of Li and Si mixing at 1200 K with Ne=0, 3/64, and 5/64 at different simulation times.

**Figure 6.** MSD of Li and Si as a function of time at temperatures 1100 K-1500 K. Inset shows the isosurface of the charge density difference for Li-Si systems with and without extra electrons.

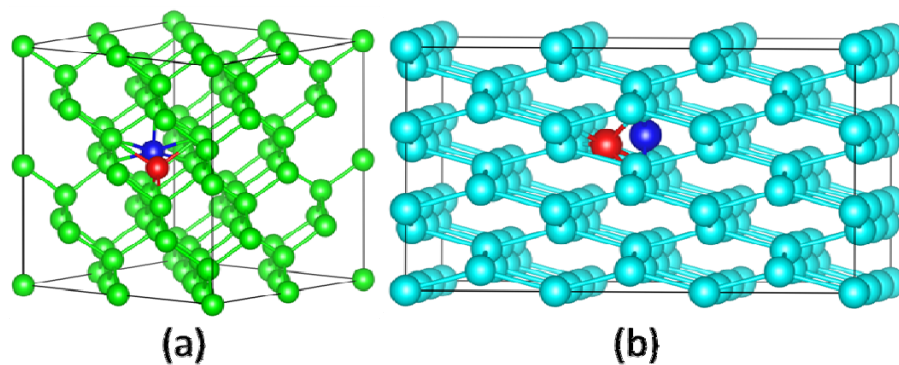
**Figure 7.** Diffusivity of (a) Li and (b) Si with respect to the inverse of temperature. The value of diffusivity is extrapolated to low temperatures using an exponential fit.

Figure 1

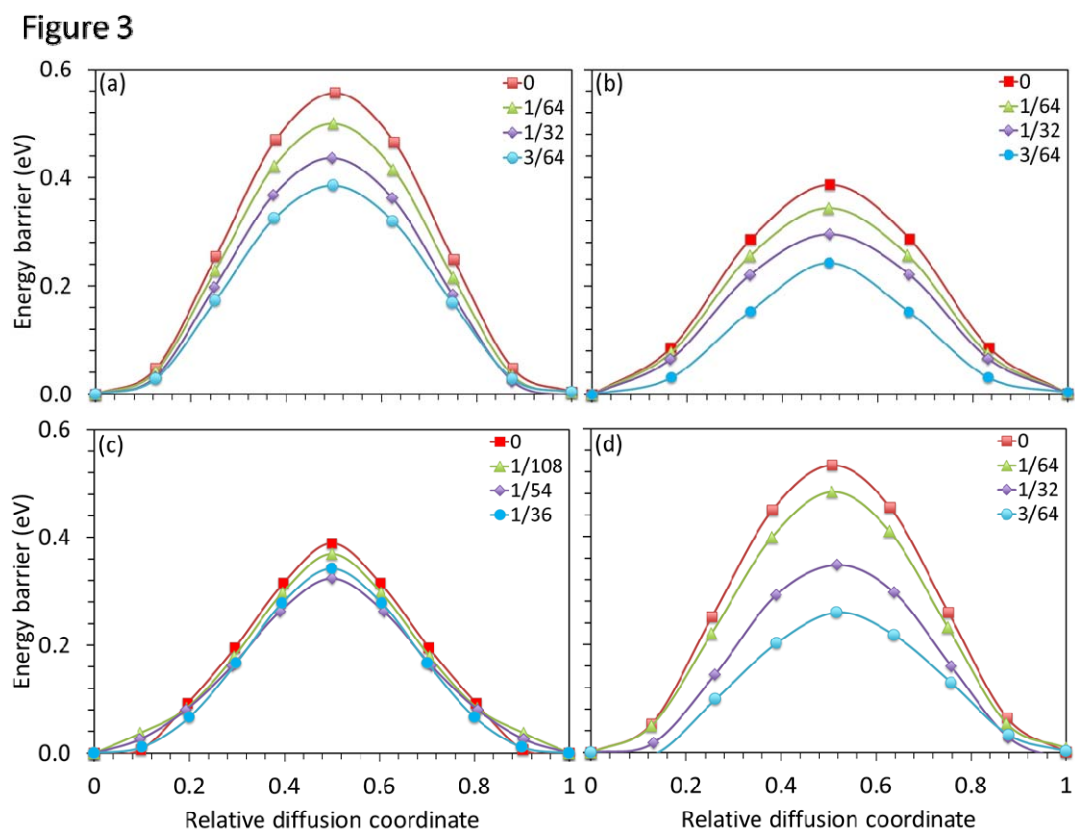


**Figure 1.** (a) STEM Z-contrast image, Li maps, Si maps, and Li/Si composite maps showing the distribution of Li and Si in different lithiation stages<sup>17</sup>. (b) Schematic drawing illustrating the distribution of Li and electrons during lithiation based on interface-controlled lithiation theory. Due to the interface-controlled lithiation process, Li accumulates at the interface and forms a Li<sup>+</sup> rich interface, while electrons are rich in the silicon core.

Figure 2

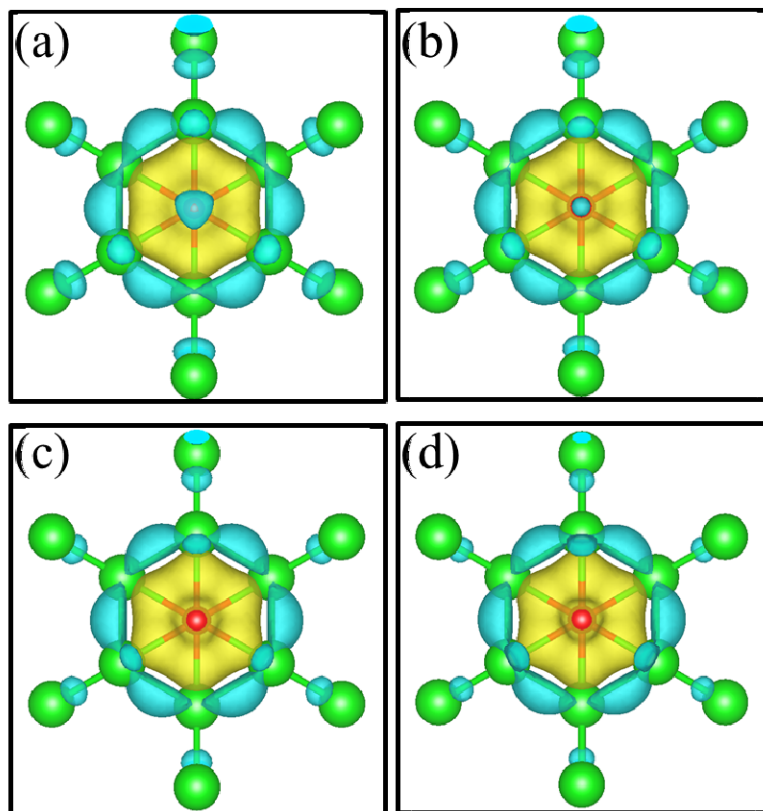


**Figure 2.** Atomic structures of diamond (a) Si and Ge, and (b) body centered tetragonal Sn. The green ball represents Si and Ge atoms. Cyan ball represents Sn. Red and blue balls represent the stable and transition state of Li atoms, respectively.

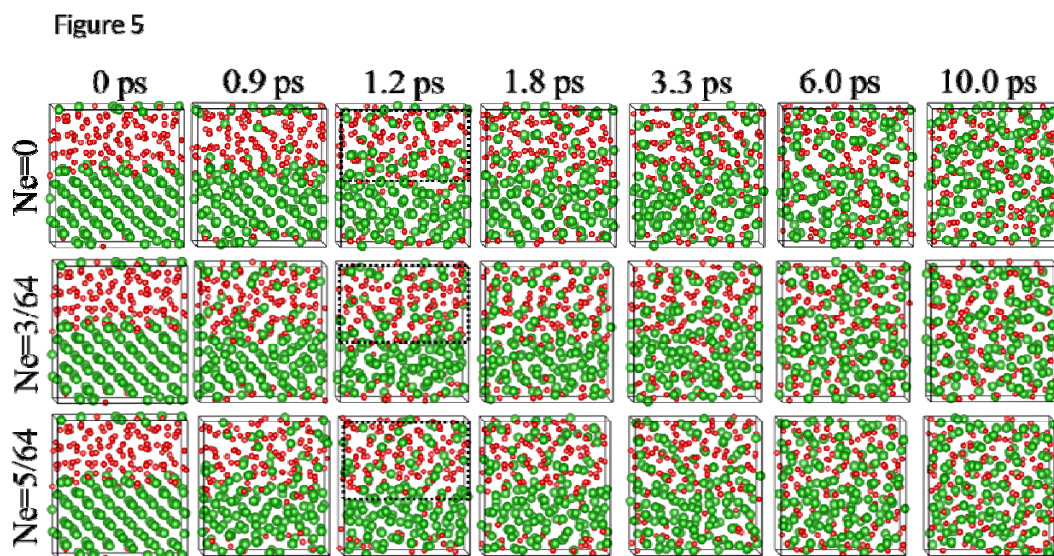


**Figure 3.** Energy profiles of Li diffuse in (a) pristine Si, (b) pristine Ge, (c) pristine Sn, and (d) P-doped Si with and without adding additional electron on the systems.

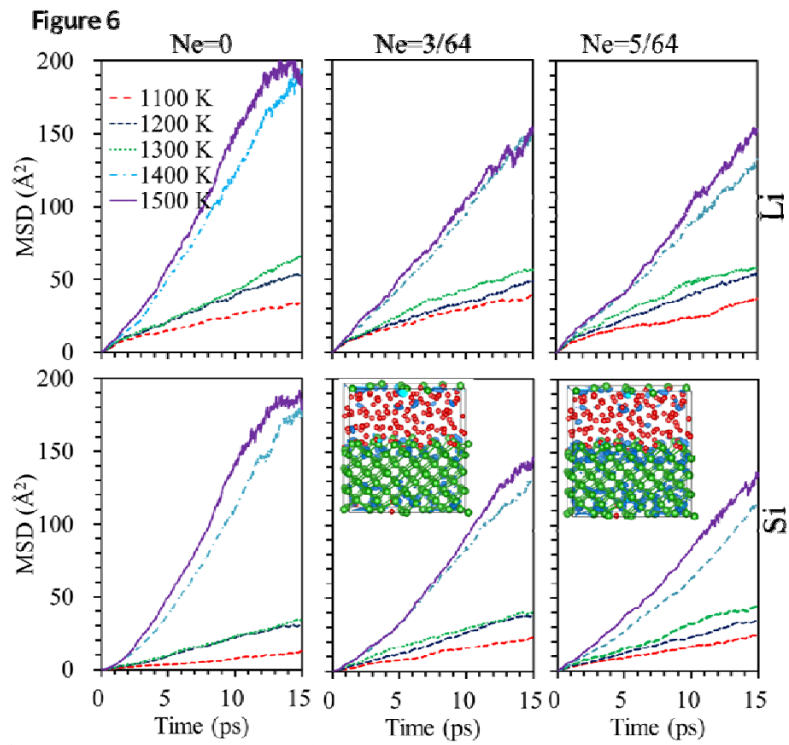
Figure 4



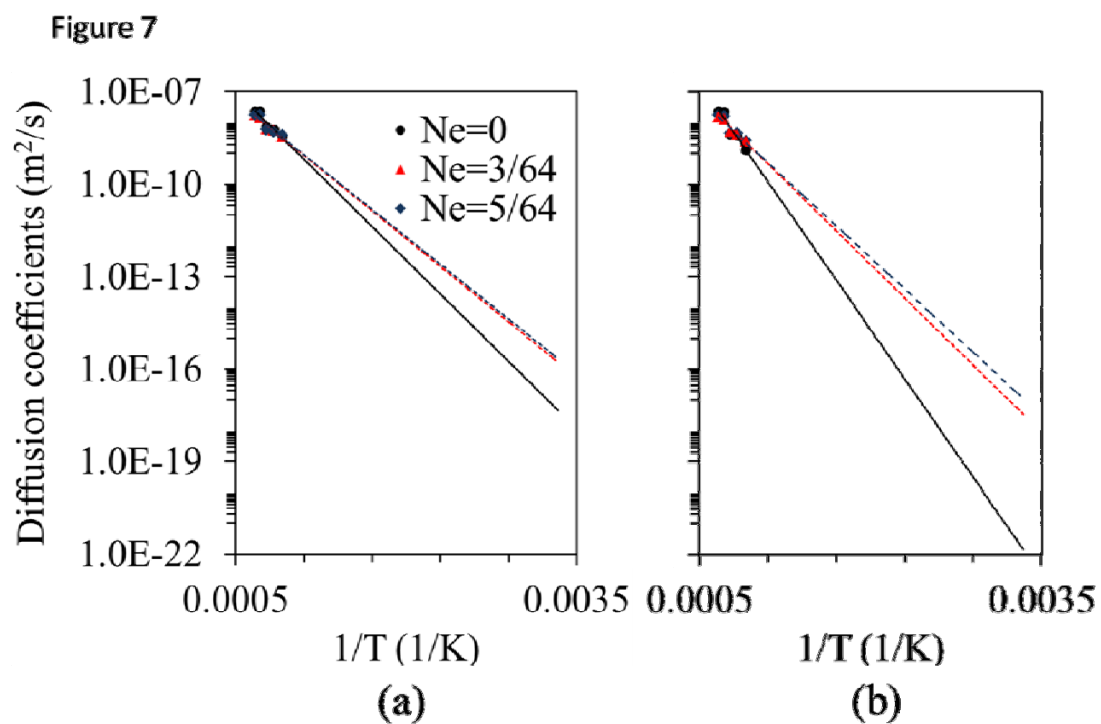
**Figure 4.** Isosurface of the charge density difference for Li located at saddle (Hex) site ( $0.0008 \text{ e}/\text{\AA}^3$ ) with adding additional electron of Ne=(a) 0, (b)  $1/64$ , (c)  $1/32$ , and (d)  $3/64$ . Yellow surfaces correspond to charge gains and cyan surfaces correspond to an equivalent charge lost.



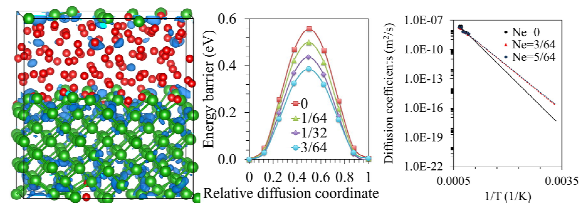
**Figure 5.** Structural snapshots of Li and Si mixing at 1200 K with Ne=0, 3/64, and 5/64 at different simulation times.



**Figure 6.** MSD of Li and Si as a function of time at temperatures 1100 K-1500 K. Inset shows the isosurface of the charge density difference for Li-Si systems with and without extra electrons.



**Figure 7.** Diffusivity of (a) Li and (b) Si with respect to the inverse of temperature. The value of diffusivity is extrapolated to low temperatures using an exponential fit.



Enhancement of Lithium Diffusion by Electron-Rich Effect in Group IVA Elements for Lithium Ion Batteries.